Journal for ImmunoTherapy of Cancer

Intratumor expanded T cell clones can be non-sentinel lymph node derived in breast cancer revealed by single-cell immune profiling

Shiping Jiao ,[1] Qing Xiong,[1] Meisi Yan,[2] Xiaolu Zhan,[3] Zhenhuang Yang,[1] Cheng Peng,[1] Beicheng Sun,[1] Da Pang,[3,4,5] Tong Liu[3,4]

To cite: Jiao S, Xiong Q, Yan M, *et al*. Intratumor expanded T cell clones can be non-sentinel lymph node derived in breast cancer revealed by single-cell immune profiling. *Journal for ImmunoTherapy of Cancer* 2022;**10**:e003325. doi:10.1136/jitc-2021-003325

► Additional supplemental material is published online only. To view, please visit the journal online (http://dx.doi.org/10.1136/jitc-2021-003325).

1

Accepted 23 November 2021

For numbered affiliations see end of article.

Correspondence to
Dr Tong Liu;
liutong@hrbmu.edu.cn

Dr Da Pang;
pangda@ems.hrbmu.edu.cn

Dr Shiping Jiao;
jiaoshp@tcrximmune.cn

ABSTRACT

Background Sentinel lymph nodes (LNs) are regarded as key immune surveillance sites in cancer wherein mature dendritic cells present tumor-derived antigens to prime and activate T cells, which then migrate to the tumor site. However, it is unclear whether the tumor-specific T cells can be elicited within the tumor independent of the sentinel LNs.

Methods We performed an integrative analysis of gene expression profiles of 65,285 cells and T cell receptor sequences of 15,831 T cells from 5 paired primary breast tumors and sentinel LNs to identify where clonal T cells come from and the characteristics of those clonal T cells.

Results The proportion of clonal T cells was higher in the primary tumors compared with the sentinel LNs, whereas all expanded clones identified in the sentinel LN were also present in the primary tumors. In contrast, 10.91% of the expanded clones in the primary tumors were not found in the sentinel LNs. These novel intratumoral T cell clones were characterized by high tissues retention capacity (CXCR6 +ITGAE+) and a distinct coinhibitory pattern (CD39 +NKG2A+) compared with the expanded T cell clones common to both sites. Furthermore, multiplex immunofluorescence imaging showed the presence of tertiary lymphoid structures (TLS) in the primary breast tumors wherein the activated cytolytic T cells were concentrated, indicating its possible role in eliciting non-sentinel LN-derived T cell clones.

Conclusions Our study revealed expanded intratumor non-sentinel LN derived T cell clones located in the TLS, which points to the need for exploring the role of TLS in antitumor immunity.

BACKGROUND

The accumulation of mutations in cancer cells generate tumor-specific antigens that elicit the host immune response.[1] The antigens shed from the tumor cells are captured by the mature dendritic cells (DCs), which then migrate to secondary lymphoid organs and present the antigenic peptides with the major histocompatibility complex to T cells and B cells. Following antigen recognition, the CD4 +T cells promote B cell proliferation in the primary follicles to form a secondary follicle as germinal center, wherein the primed and activated lymphocytes can expand further. The antigen-primed T cells and B cells eventually egress from the lymph node (LN) and enter the tumor bed.[2] However, it is unclear whether these tumor-specific T cell clones are primed only within the sentinel LNs and then migrate to the tumor, or if a proportion of expanded clones can be primed and elicited within the primary tumor sites.

Tertiary lymphoid structures (TLS) in tumors have drawn considerable interest in recent years as a proxy for an immunologically 'hot' environment. Studies show that TLS play a major role in controlling tumor invasion and metastasis, and a high density of TLS correlates with favorable overall survival and disease-free survival in multiple cancer types.[3] In addition, the presence of B cells and T follicular helper cells in the TLS correlates with improved prognosis in murine cancer models as well as patients.[4–6] However, the exact role of TLS, or its potential function as an LN-like structure, in antitumor immunity is unknown.

Single-cell T cell receptor (scTCR) sequencing allows rapid identification of putative antigen-specific T cell clones.[7 8] Furthermore, integrated analysis of TCR and single-cell gene expression data can help track T cell clones and their transcriptional phenotypes,[7 9] and assess the relationship of T cells in different locations.

Sentinel LN biopsy therapy is concepted and commonly applied in breast cancer surgery. It along with the removal of primary breast tumor is the standard treatment for most, clinically node-negative breast cancer at diagnosis who undergoes conservative surgery as initial treatment.[10] In addition,

in the breast cancer mastectomy, the primary breast cancer and the corresponding sentinel LN are easy to be exposed by the surgeons and yield a clear anatomic relationship particularly with the aid of staining dye. These clinical features provided us the opportunity to collect the primary tumors and the first tumor draining LNs. In this study, we collected primary breast cancer tissues and adjacent sentinel LNs from 5 patients, and performed single cell gene expression profiling and TCR sequencing to determine the relationship between intratumoral and sentinel LN-residing T cell clones.

MATERIALS AND METHODS

Clinical subjects and clinical sample collection

Five patients with clinically node-negative breast cancer at diagnosis who undergoes conservative surgery as initial treatment were recruited from Harbin Medical University Cancer Hospital. The demographic characteristics of the study population are listed in online supplemental table S1.

Sentinel LN identification and collection

A blue dye was injected close to the tumor, and the stained sentinel LNs were detected after 15 min using a probe. All sentinel LNs (generally 4–6) were collected from each of the 5 patients.

Generation of single cell RNA-seq and V(D)J libraries

The single cell RNA-seq and V(D)J libraries were generated using the 10X Genomics Chromium Controller Instrument and Chromium single cell 5' library & gel bead kit, and the V(D)J enrichment kit according to manufacturers' instructions. Briefly, 8000 peripheral blood mononuclear cells (PBMCs) (>90% viability) were loaded on the controller to generate single-cell gel bead-in-emulsions. The mRNA was reverse transcribed and sample indexed to barcoded cDNA, purified using DynaBeads and amplified by PCR. To construct the 5' gene expression library, the amplified barcoded cDNA was fragmented, end repaired, A-tailed, sample indexed and double-sized selected with SPRI beads (average size 450 bp). For the V(D)J library, human T cell V(D)J sequences were enriched from the amplified cDNA followed by fragmentation, end repairing, A-tailing, sample indexing and double-sized selection with SPRI beads (average size, 600 bp). The DNA was quantified, and fragment size distribution of the libraries were determined using the Qubit dsDNA HS assay kit (Thermo, Q32851) and Agilent 2100 BioAnalyzer High Sensitivity DNA kit (Agilent Technologies, 5067-4626). Pooled libraries were then sequenced on an Illumina high output sequencing platform, with 150 bp on the two reads for RNA-seq and V(D)J libraries.

10X library sequencing

The single-cell RNA libraries were sequenced on an Illumina Novaseq to a minimum sequencing depth of 50 000 reads per cell using reads lengths of 150 bp read 1, 8 bp i7 index and 150 bp read 2. The scTCR libraries were sequenced on an Illumina Novaseq to a minimum sequencing depth of 10 000 reads per cell using reads lengths of 150 bp read 1, 8 bp i7 index and 150 bp read 2. For scRNA-seq, 86,401 cells and 7,168,372,158 reads were obtained with an average of 716,837,216 reads per sample and 82,966 reads per cell, and an average of 19,345 genes were detected per sample. For scTCR-seq, 38,429 cells and 582,432,249 reads were obtained with an average of 58,243,225 reads per sample and 15,156 reads per cell. The single cell mapping statistics are shown in online supplemental table S2.

Analyses of scRNA-seq data

The scRNA-seq reads of each sample were independently aligned to the GRCh38 reference genome (10X Genomics, V.3.0.0) and quantified using cellranger count pipeline (10X Genomics, V.3.1.0) with default parameters. Filtered count matrix of features generated from cellranger count were then analyzed using Seurat (V.3.1.5).[11] Genes expressed in <3 cells, cells with <200 or >5000 expressed genes, or cells with >10% mitochondrial counts were discarded. As described by Yost *et al*[12] batch effects between samples and cells related to S and G2/M cell cycle phases, heat-shock gene expression signature, number of unique molecular identifiers (UMIs) per cell and mitochondrial RNA content were removed when scaling the data. Variable genes were identified based on average of expression >0.1 and dispersion >1, and the top 5000 variable genes were analyzed. To avoid clustering based on variable V(D)J transcripts, the variable TCR and immunoglobulin genes were not included. In addition, the S and G2/M cell cycle and heat-shock signature genes were also removed to prevent any clustering effect due to both factors. Cells were clustered using a shared nearest neighbor modularity optimization-based clustering algorithm with the first 50 principal components and resolution set to 0.5. The clusters were annotated manually based on the differentially expressed genes (DEGs) between clusters (online supplemental tables S3,S4). The differential expression test was performed by FindAllMarkers function in the Seurat package with min.pct=0.25, other parameters as default, and only positive markers (only.pos=TRUE). Wilcoxon rank-sSum test was used for statistical analysis.

Analyses of scTCR-seq

The scTCR-seq reads were independently aligned to the GRCh38 reference genome (10X Genomics, V.3.1.0) for each sample, and the clonotype analysis and TCR annotation were performed using the cellranger VDJ pipeline (10X Genomics, V.3.1.0). The percentage of clonotypes in each sample is calculated as: cells with identical T cell receptor beta locus (TRB) CDR3/total T cells * 100%.[9]

Velocity analysis of malignant cells

RNA velocity is defined as the rate of change of mRNA molecule abundance in the cell.[13 14] The cancer cell clusters 9, 12, 16, 18, 19, 22, and 25 with respective cell numbers

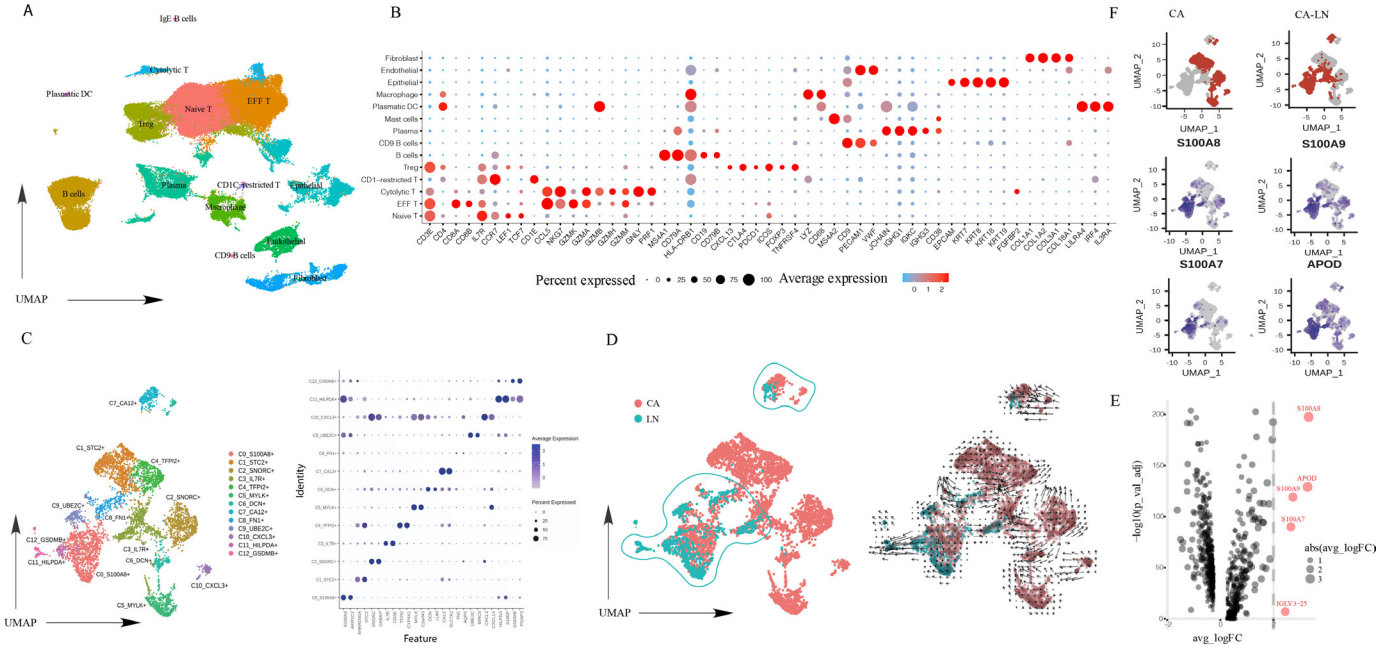

Figure 1 Primary cancer cells inclined to metastasis express high levels of S100A and APOD. (A) UMAP of all cells with each cell type indicated by a color code. (B) Expression of characteristic markers in each cell type. (C) UMAP of malignant cells with color-coded clusters and expression of characteristic genes in each cluster. (D) UMAP of malignant cells from CA (red) and LN (blue), and the velocities (arrows) of malignant cell. (E) Volcano plot of DEGs. Differential expression test was perform by Wilcoxon rank sum test. Significant DEGs with p<0.05 and absolute value of avg_logFC≥2 are indicated in red. (F) Distribution of cancer cells in the pure (CA) and mixed (CA & LN) areas in the UMAP space and the expression of four DEGs. avg_logFC, log fold-chage of the average expression between the two groups; CA, cancer; DC, dendritic cell; DEGs, differentially expressed genes; LN, lymph node; UMAP, uniform manifold approximation and projection.

1957, 1600, 1035, 445, 300, 140 and 98 were extracted and re-clustered to get higher resolution. Using the optimal resolution of 0.4, 13 clusters were obtained (figure 1) and velocity analysis was performed by velocyto[14] (python version) with default parameters. The DEGs were identified by FindMarkers function in the Seurat package with default parameters using primary cancer cells with (C0, C3, C7, C8, C9, C11, C12) and without (C1, C2, C4, C5, C6, C10) migration tendency. The DEGs were visualized by the volcano plot, and the thresholds were p<0.05 and avg_logFC≥2.

Velocity analysis of T cells

The velocity analysis of T cells was performed using scVelo.[13] The parameters were set as follows: counts=20, n_top_genes=2000, n_pcs=30 and n_neighbors=30.

CNV analysis and identification of malignant cells

Since most breast cancers are carcinomas that arise from the epithelial cells,[15] the epithelial gene signature was constructed using the top 50 genes with highest correlation to epithelial cell adhesion molecule (EPCAM), and clusters 9, 12, 16, 18, 19, 22 and 25 were annotated by the module scores of these genes. The enrichment of epithelial signature genes in individual cells were scored using the function AddModuleScore in Seurat. The copy number variation (CNV) status of all cells in the epithelial clusters were inferred by R package InferCNV[16] (https://github.com/broadinstitute/inferCNV) against that of the non-epithelial cells including fibroblasts, endothelial and immune cells. Cluster specific CNVs in malignant cells were visualized by heat maps (online supplemental figure S1E,F), and the malignant and non-malignant cells were distinguished on the basis of their individual CNV score, which was defined as the mean of squared CNV values from hidden Markov model CNV predictions across all genes for each cell. The malignant cells were defined as those with CNV score greater than the maximum CNV score of normal cells.

Multiplex immunofluorescence assays

Multiplex staining was performed using the Opal 4-Color Manual IHC Kit (NEL810001KT) with the anti-CD3 (1:150; ZA-0508, ZSGB-BIO), anti-CD20 (1:100; ZM-0039, ZSGB-BIO), anti-CCL4 (1:50, PA5-23681, ThermoFisher), anti-CD8 (1:100, ab4055, abcam), anti-PNAD (1:100, #120801, Biolegend), anti-PD1(1:100, ab52587, Abcam) and anti-CD103 (1:100, ab254017, Abcam) antibodies with subsequent visualization with fluorescein AF-690 (1:75), AF-520 (1:75) and AF-570 (1:50). The nuclei were counterstained with 4', 6-diamidino-2-phenylindole (1:3,000). All sections were covered with Vectashield Hardset 895 mounting media, and scanned using the Vectra slide scanner (PerkinElmer).

TCR T construction

T cells were isolated from peripheral blood mononuclear cells from the patient by CD3/CD28 bead pulldown and

incubated overnight with CD3/CD28 antibody-coated beads in the presence of 100 units/mL rh interleukin-2. Activated T cells were lentivirally transduced to express the patient-derived TCR sequences or vector control, as previously described.[8] The VDJ sequences of transduced TCR sequence were derived from the patient's four expanded T cell clones or four clones represented by only one cell. The mouse TCR alpha and beta constant domains were utilized to construct the full length of TCR to decrease the possibility of mispairing with endogenous TCR alpha or beta chains. The transduced T cells expanded for 5 days.

INTERFERON Γ ELISA

The 96-well plate was coated with interferon γ (IFNγ) capture antibody for 48 hours. A total of 1×10^5 TCR-T cells per well cultured with 2×10^5 autologous tumor cells (1×105) for 24 hours in the plate. Supernatants were collected and analyzed for IFNγ using the Human IFNγ DuoSet ELISA (R&D Systems), with the use of a luminescent HRP substrate (Glo Substrate, R&D Systems). The signal was measured using the FLUOstar Omega plate reader (BMG Labtech).

RESULTS

Cell-type composition in primary breast cancers and paired sentinel LN

Single cell suspensions of primary breast tumors and paired sentinel LNs of 5 patients (P1–P5) were prepared (figure 2A and online supplemental table S1). All patients had histologically confirmed tumors, and metastatic cancer cells were detected in at least one sentinel LN of each patient (figure 2B and online supplemental table S1). Single cell gene expression analysis and TCR sequencing were performed using the 10X genomics platform. After quality control (online supplemental figure S1A,B), 32,923 cells from the tumor tissues and 32,362 cells from the corresponding sentinel LNs were clustered into 27 clusters (online supplemental figure S1C) and annotated as 14 subsets: Naïve T cells (CD3E+, IL7R+, CCR7+), effector (EFF) T cells (CD3E+, CCL5+, NKG7+, GZMK+, GZMA+), Cytolytic T cells (FGFBP2+, NKG7+, GZMA+, GZMB+, GZMM+, GNLY+, PRF1+, CCL5+), CD1-restricted T cells (CD1E+, CCR7+, IL7R+), Treg cells (CD4+, FOXP3+, TNFRSF4+, CTLA4+), B cells (CD19+, MS4A1+, HLA-DRB1+), CD9 B cells (CD9+, PECAM1+), Plasma cells (JCHAIN+, IGHG1+, IGKC+, CD38+, CD19-), Mast cells (MS4A2+), Plasmatic DCs (LILRA4+, IRF4+, IL3RA+), Macrophage (CD68+, HLA-DRB1+, LYZ+), Epithelial cells (EPCAM+, KRT7+, KRT8+, KRT18+, KRT19+), Endothelial cells (PECAM1+, VWF+), and Fibroblasts (COL1A1+, COL1A2+, COL3A1+, COL18A1+) (figure 1A,B). All 14 subsets were identified in breast tumors and the sentinel LNs. The proportion of antigen-experienced T cells (EFF T cells and cytolytic T cells) were higher in tumors, whereas B cells were more abundant in the LNs (online supplemental figure S1C,D). This is consistent with the large number of B cells

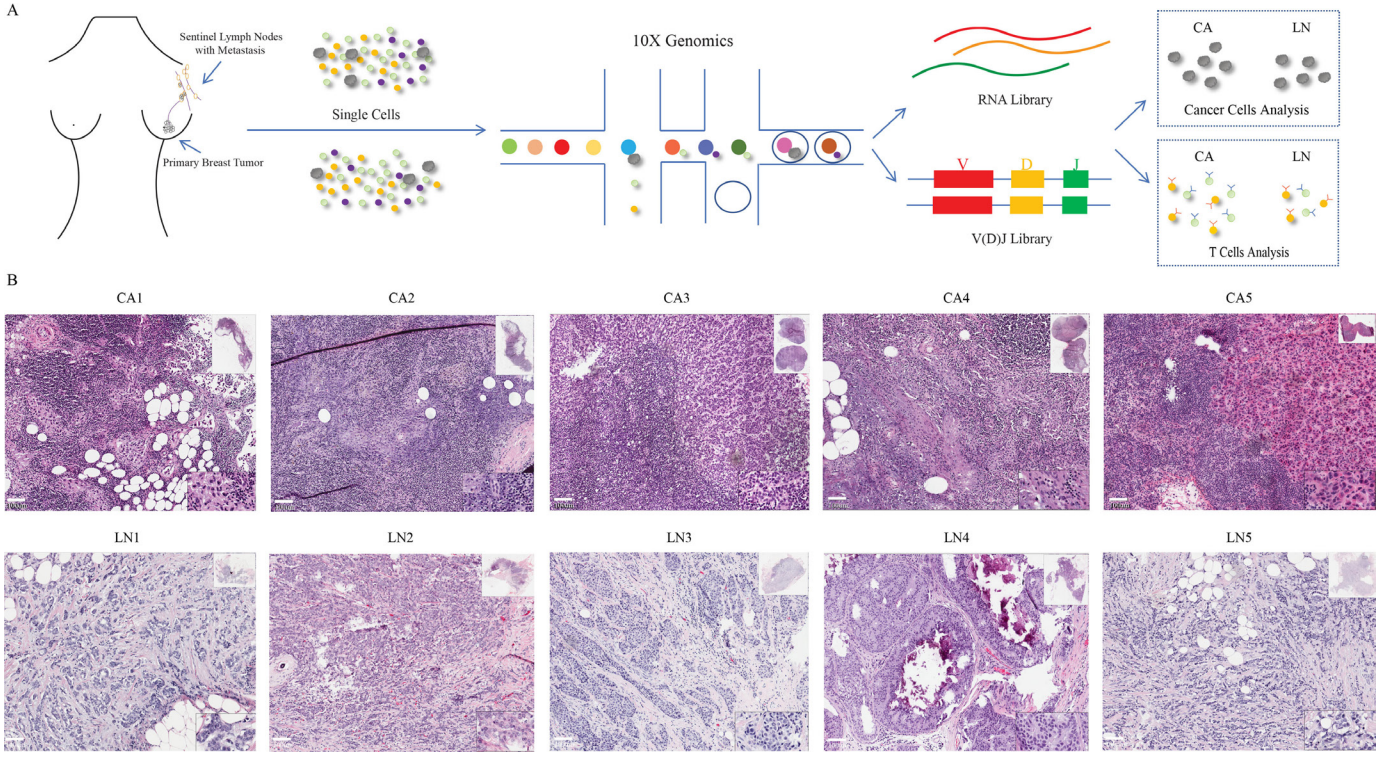

Figure 2 Single-cell RNA and TCR analysis of primary breast tumors and paired sentinel LNs of 5 patients. (A) Schematic illustration of the analyses performed in this study. (B) Representative images of HE-stained primary breast tumors and sentinel LNs of 5 patients. LN, lymph node; TCR, T cell receptor.

observed in the germinal centers of LNs, and the enrichment of antigen-experienced T cells in the tumor sites.

Primary breast cancer cells inclined to metastasis express high levels of S100A and APOD

Studies show that CNV patterns can be used to distinguish between the malignant and non-malignant cells.[9 17 18] We calculated a CNV score for each cell and used this score to distinguish the malignant cells from non-malignant cells. We found that all 27 clusters (online supplemental figure S1C) contained exclusively malignant or non-malignant cells, and the epithelial clusters are pure malignant cells. This is consistent with another study's finding that epithelial and CNV-based classifications were highly concordant and cross-validated.[17]

The identified malignant cells from tumor tissues and sentinel LNs were reclustered into 13 subsets (figure 1C). The clusters C1, C2, C4, C5, C6 and C10 were mainly composed of cancer cells from primary tumor sites (CA area), while clusters C0, C3, C7, C8, C9, C11 and C12 consisted of cancer cells from both CA & LN areas (figure 1D and online supplemental figure S1G). The proximity between the mixed CA & LN primary cancer cells and metastatic cancer cells on the uniform manifold approximation and projection (UMAP) indicated their high transcriptomic similarity. RNA velocity analysis showed a trend that cancer cells in primary tumors concentratedly pointed to those in LNs (figure 1D), indicating that these cancer cells would likely develop to the status of those in the sentinel LNs. In contrast, the velocity directions in the pure primary cancer cell populations were diverse. This indicates that the primary cancer cells in the mixed area are more inclined to metastasize to the LNs. Finally, differential gene expression analysis between metastasis-inclined cancer cells and those of CA areas showed that S100A7, 8 and 9 and APOD were significantly upregulated in the metastasis-inclined cancer cells, with S100A8 (avg_logFC=3.32, p_val_adj=3.02E-198) exhibiting the maximum increase in expression levels (figure 1E,F). It has been documented that S100A7, S100A8, and S100A9 are key molecules in cell motility and promote the migration and metastasis of multiple cancers.[19 20] APOD has been found to confer an increased risk of developing metastatic breast cancers.[20]

Characteristics of T cells residing in primary breast cancers and paired sentinel LNs

We further profiled the T cells residing within the tumors and in paired sentinel LNs with metastasis. A total of 15 831 T cells with both transcriptome and TCR information from tumor tissues (8665 cells) and paired sentinel LNs (7166 cells) of 5 breast cancer patients were batch-effect corrected (online supplemental figure S2A,B) and clustered into 11 clusters (figure 3A). Clusters 4, 1, 3 and 5 were annotated as Naïve T cells (LEF1+, CCR7+, TCF7+), Naïve EFF T cells (CCR7+, TCF7+, CD69+), Treg cells (CD4+, FOXP3+, CD25+, ICOS+, CTLA4+) and T follicular cells (CD4+, TOX+, CXCL13+, PDCD1+, ICOS+) (figure 3C, online supplemental table S3). Naïve T cells and Naïve EFF T cells mainly comprised of CD4 T cells along with a small proportion of CD8 T cells. Cluster 10 was characterized by high expression levels of the cytotoxic granules granzyme B (GZMB), granzyme A (GZMA), granzyme H (GZMH), perforin 1 (PRF1) and granulysin (GNLY), and very low levels of inhibitory molecules. Cluster 10 was annotated as Cytolytic T cells with strong cytotoxic capacity. Cluster 9 also expressed high levels of cytotoxic granules but had lower GZMA, PRF1 and GNLY expression compared with cluster 10. In addition, cluster 9 also expressed the co-inhibitory molecules programmed cell death 1 (PDCD1), hepatitis A virus cellular receptor 2 (HAVCR2), T cell immunoreceptor with Ig and ITIM domains (TIGIT), cytotoxic T-lymphocyte associated protein 4 (CTLA4) and lymphocyte activating 3 (LAG3), which was indicative of a dysfunctional or inclined to dysfunctional status. Therefore, we annotated this cluster as dysfunctional T cells.

The majority of CD8 T cells (clusters 0, 2, 6, 7 and 8) were antigen experienced, as indicated by the presence of CD69+, CCL5 +and NKG7+, and mainly expressed GZMK. In contrast, the GZMB, GZMH, PRF1 and GNLY levels in these antigen-experienced T cells were significantly lower compared with those in Cytolytic T cells and Dysfunctional T cells. To further explore the plasticity of antigen-experienced T cells, we performed a velocity analysis.[13 14] RNA velocities (arrows) of all T cells were projected and visualized in the UMAP space (figure 3B). Cells in cluster 8 flowed to either cluster 9 (dysfunctional T cells) or cluster 10 (cytolytic T cells). The antigen-experienced T cells (clusters 0, 2, 6, 7, 8) contained several 'velocity centers' that pointed to different cell states like cytolytic, dysfunctional or naive, indicating a high plasticity of this population. Therefore, we annotated this population as plastic transitional EFF T cells.

The CD8 +T cells were then plotted on the diffusion map and the clustering information of UMAP was integrated. The Cytolytic T cells, Dysfunction T cells and Naïve T cells were consistently aggregated into three separate branches (figure 3D), indicating their divergent status. The plastic Transitional EFF T cells (clusters 0, 2, 6, 7 and 8) were aggregated in the intersection of the three branches. To further identify potential markers of the functional status of the intratumoral and sentinel LN T cells, we analyzed the average expression levels of naïve, cytolytic and dysfunctional status-related makers in cells along the first or second component of the diffusion map (figure 3E). All candidate markers were selected from the list of DEGs (online supplemental table S4). As shown in figure 3F, fibroblast growth factor binding protein 2 (FGFBP2), HAVCR2 and lymphoid enhancer binding factor 1 (LEF1) were specific to the cytolytic, dysfunctional, and naïve populations. The activation and exhaustion scores of the cells were next calculated based on the respective signature genes that showed correlation to FGFBP2 (activation) and HAVCR2 (exhaustion). We plotted the expression of FGFBP2, HAVCR2 and LEF1

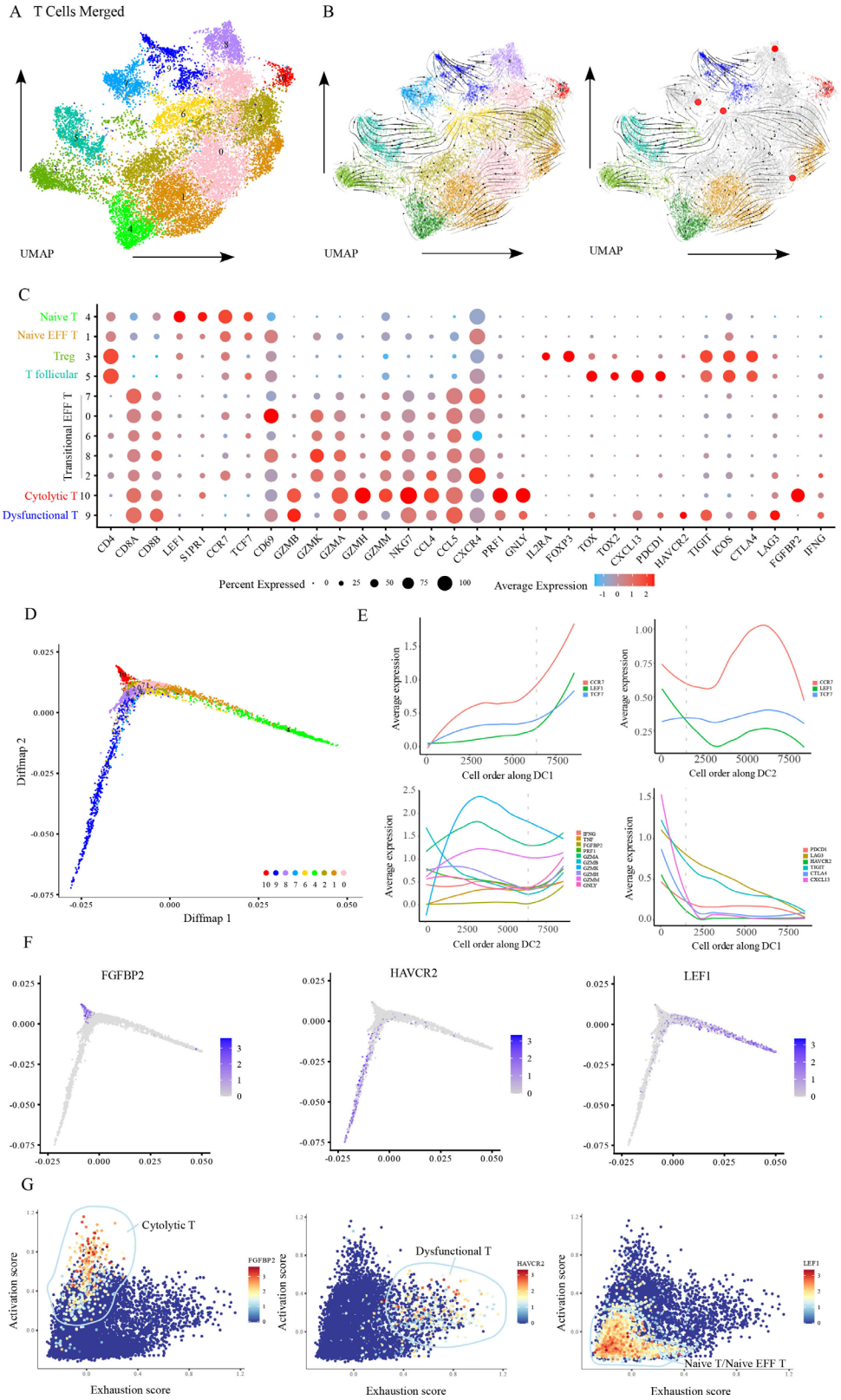

Figure 3 Characteristics of T cells residing in primary breast cancers and paired sentinel LNs. (A) UMAP of T cells with color-coded clusters. (B) Velocities (arrows) of T cells in the different clusters. (C) Expression of characteristics genes in each T cell subset. (D) Diffusion map of all CD8 +T cells. (E) Average expression of naïve, cytolytic and exhaustion markers across diffusion component one and diffusion component 2. (F) Diffusion map of cytolytic (FGFBP2), exhaustion (HAVCR2) and naïve (LEF1) markers. (G) Scatter plots of T cells in the space of activation and exhaustion scores color-coded by expression levels of FGFBP2, HAVCR2 and LEF1. DC, dendritic cell; FGFBP2, fibroblast growth factor binding protein 2; HAVCR2, hepatitis A virus cellular receptor 2; LEF1, lymphoid enhancer binding factor 1; LN, lymph node; UMAP, uniform manifold approximation and projection.

into the space of T cell activation-exhaustion, and found that they represented the cytolytic, dysfunctional, and naive status of cells (figure 3G).

Cytolytic T cell population showed the strongest expansion, migration and transition capacity

Integrated analysis of the single-cell gene expression levels and TCR seq of intratumoral and sentinel LN T cells showed clonal expansion of multiple TCR clonotypes located in the antigen-experienced T cell area in the UMAP plot (figure 4A,B). The clonal expansion was defined as that the proportion of T cells with identical TRB CDR3 sequences in total T cells of the sample is larger than 1%, which are also most likely to be tumor-reactive T cells.[7 9] All the identified clonally expanded T cells were CD8 +T cells, and the intratumoral T cells showed greater clonality compared with those in sentinel LNs (figure 4B). When compared the clonotype sharing between primary tumor sites and corresponding sentinel LN, we found a large number of overlapping clonotypes in antigen-experienced T cells, Treg and T follicular cells population of these two sites, while in Naïve and Naïve EFF T cell populations, the clonotype sharing is much less (figure 4C,E). In addition, we found that most of expanded clones were common to the primary tumors and sentinel LNs, and all expanded clones in the latter were also identified within the tumor (figure 4D), which is consistent with the hypothesis that antitumor T cells are primed in the sentinel LNs before migration to primary tumors.

STARTRAC was performed to check the degree of clonal expansion, tissue migration and transition states of the T cell subsets in terms of the expa, migr and tran indices respectively.[21] We found that the cytolytic T cell population showed the most significant expansion, migration and transition ability (figure 4F), indicating that these cells may constitute the most active antitumor T cell population.

Intratumoral dominant cancer-specific T cell clones are potentially derived from non-sentinel LNs

Based on the distribution and frequencies of the clonally expanded T cell populations in tumor tissues and sentinel LNs, we classified the TRB clones into the novel, expanded, persistent and contracted types. Novel clones were only detected in primary tumors, whereas the expanded or contracted clones referred to their significant expansion and contraction in the primary tumor sites ($p<0.05$). The persistent clones had a similar abundance in both tumors and sentinel LNs, and at least one cell was detected at each site. All expanded clones in the five sentinel LN samples were also identified within their paired tumors (figure 4D). In order to show the tumor reactivity of the expanded T cell clones, we constructed eight TCR T cells of one patient, with four TCR sequences from the expanded T cell clones and another four from the clonetypes represented by only one cell (online supplemental figure S3A). We found all of the 4 TCRs of expanded T cell clones can recognize autologous tumor cells of the patient, and the tumor reactivity was not observed in the other four clonetypes as control (online supplemental figure S3B). These findings further support the hypothesis that the antigen-loaded DCs or metastatic cancer cells present the tumor antigens to prime T cells in sentinel LNs, which then migrate to the peripheral tumor site. Some expanded clones were identified as novel clones in tumors (figure 5A), indicating that the intratumoral environment can also prime and activate tumor-specific T cell clones.

The novel T cell clones in breast tumors express the coinhibitory CD39 and NKG2A

These T cell clones were then projected on the diffusion map, which revealed that a significant proportion of novel clones (32%) were located on the highly dysfunctional branch, followed by the contracted (12%), persistent (6%) and expanded clones (3%). Most of expanded clones (88%) resided in the transitional state (figure 5B,C).

The novel T cell clones were further characterized by differential gene expression analysis against the expanded, persistent and contracted clones. killer cell lectin like receptor C1 (KLRC1/NKG2A), CTLA4, C-X-C motif chemokine receptor 6 (CXCR6), ectonucleoside triphosphate diphosphohydrolase 1 (ENTPD1/CD39) and integrin subunit alpha E (ITGAE) were significantly upregulated, whereas interleukin 7 receptor (IL7R) and granzyme K (GZMK) were downregulated in the novel clones compared with the other three (figure 5D). CXCR6 and ITGAE mediate tissue retention and residence of T cells, and their high expression levels indicate that the novel clones are likely elicited in the tumor rather than the sentinel LNs. ENTPD1 (CD39) and KLRC1 (NKG2A) are inhibitory receptors expressed on the activated T cells[22 23] along with CTLA4.[24] Their high expression level in the novel clones suggests that the intratumorally elicited clones may be more dysfunctional and inhibitory compared with those in sentinel LNs. In addition, the downregulation of IL7R and GZMK genes indicates that novel clones are less likely to be long-term surviving and plastic.[25 26]

The TLS in primary breast cancer may induce intratumoral novel T cell clones

We hypothesized that the novel clonal T cells may be primed in the intratumoral lymphoid-like structures. To this end, we first analyzed differential gene expressions of expanded clonal CD8 T cells vs antigen experienced non-clonal CD8 T cells and identified C-C motif chemokine ligand 4 (CCL4) as the feature gene of the former (figure 6A). We next performed multiplex immunofluorescence imaging to locate CCL4 +CD8+T cells, which represent clonal T cells, in the primary tumors (figure 6B). We also included CD20 markers in the multiplex immunofluorescence panel to facilitate us to identify TLS. We found that CCL4 +CD8+T cells are highly

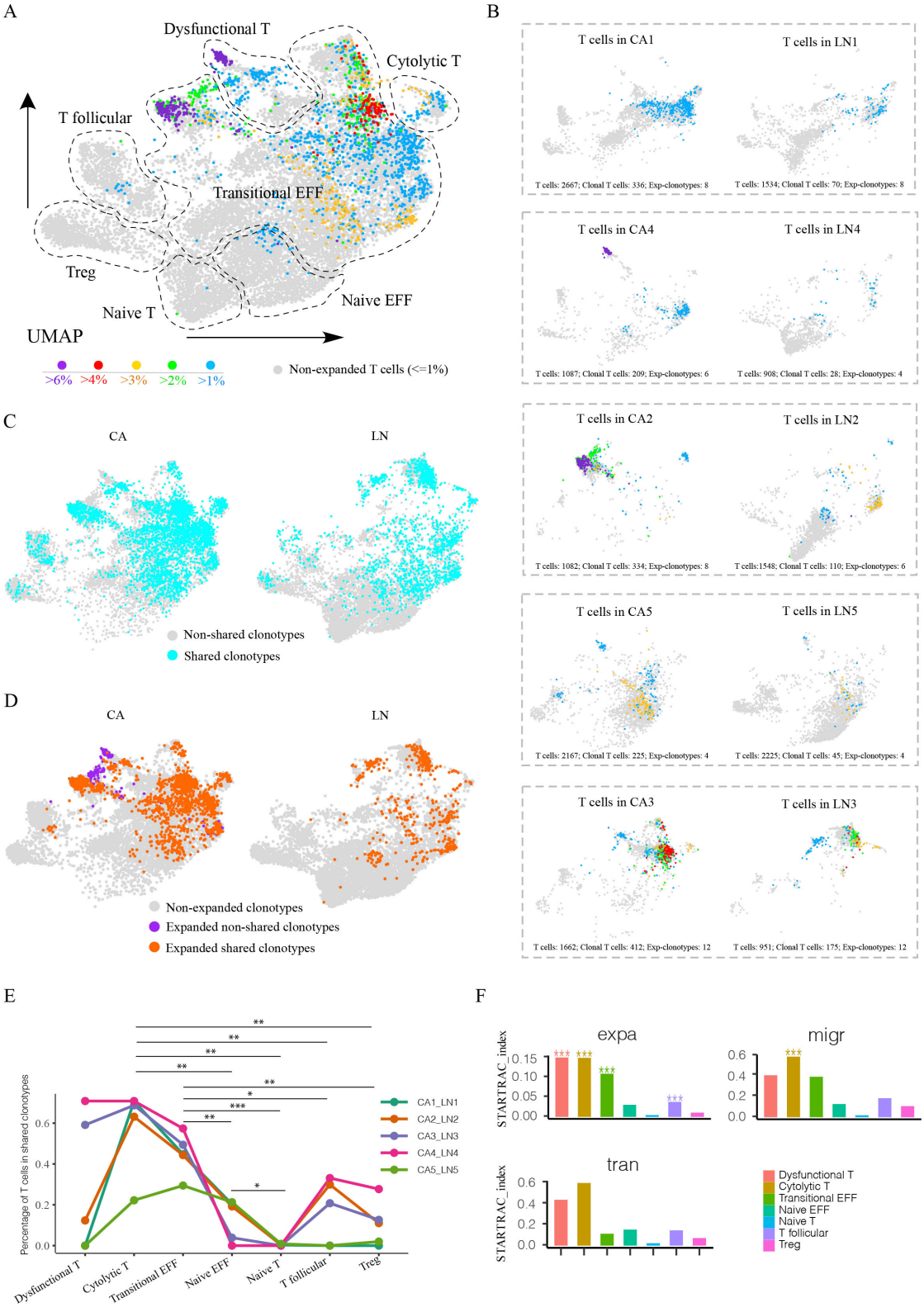

Figure 4 Cytolytic T cell population showed the strongest expansion, migration and transition capacity. (A) UMAP of T cells color-coded by percentage of TRB clonotypes. (B) UMAP of T cells from primary tumor and paired sentinel LN in each patient, color-coded by percentage of TRB clonotypes. Exp-clonotype: expanded clonotype. (C) UMAP of T cells in shared and non-shared TRB clonotypes between primary tumors and sentinel LN. (D) UMAP of T cells in shared expanded, non-shared expanded clonotypes between primary tumors and sentinel LN, and non-expanded clonotypes. (E) Percentage of T cells in shared clonotypes between primary tumors and sentinel LN for each patient in each T cell subset, significance was measured by t-test after natural log-transformed percentage values. *P<0.05, **p<0.01, ***p<0.001, respectively. (E) STARTRAC expa, migr, and tran indices of each T cell subset, ***p<0.001. CA, cancer; LN, lymph node; TRB, T cell receptor beta locus; UMAP, uniform manifold approximation and projection.

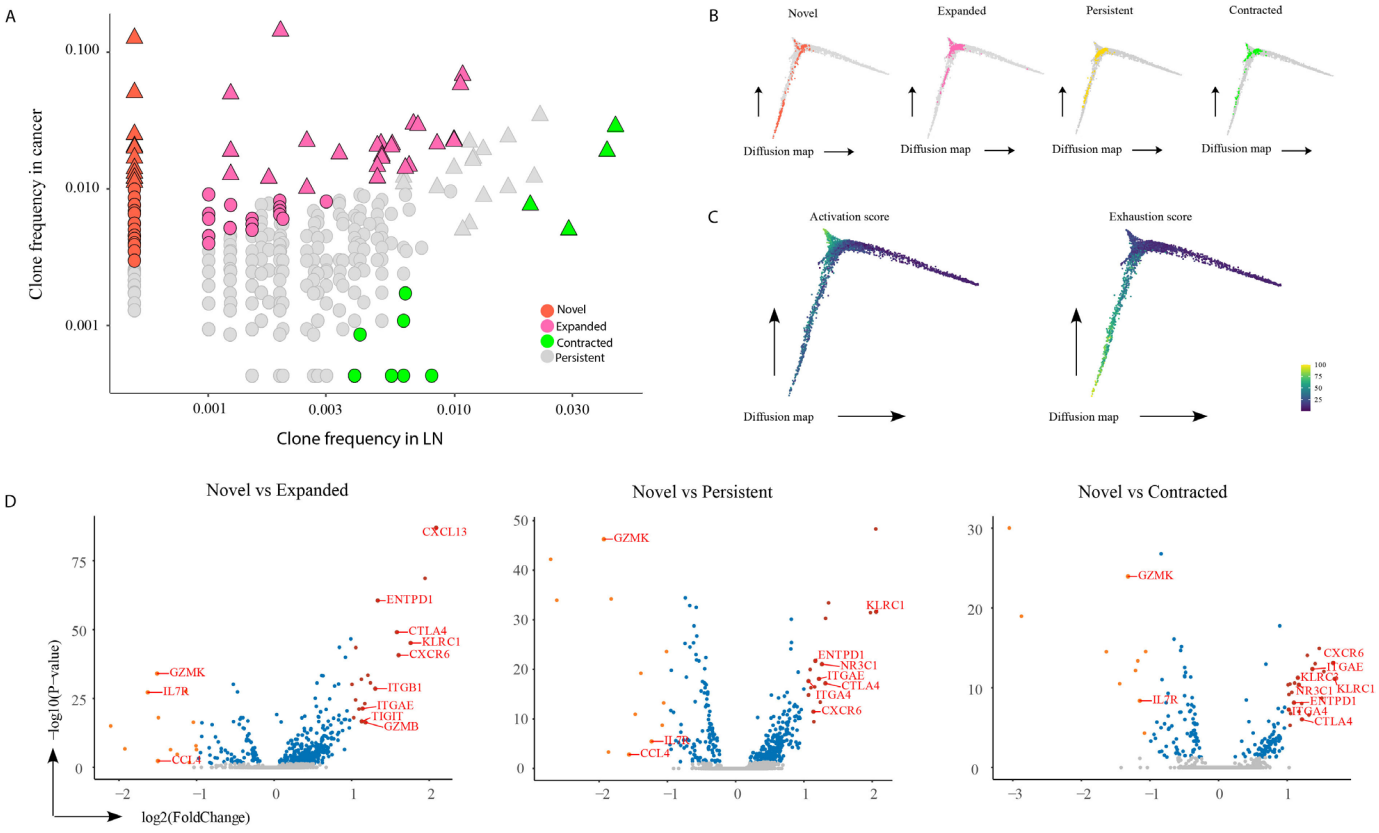

Figure 5 Intratumoral dominant cancer-specific T cell clones are potentially derived from non-sentinel LNs. (A) Frequencies of novel, expanded, persistent, and contracted clones; clones with TRB frequency >0.01 in tumors or sentinel LN are marked as triangle, others as circle. (B) Diffusion map of novel, expanded, persistent and contracted clones. (C) Diffusion map of activation and exhaustion scores. (D) Differentially expressed genes between novel and expanded, persistent and contracted clones. Significant DEGs were screened by p<0.05 and avg_FC>=2. DEGs, differentially expressed genes; LN, lymph nodes; TRB, T cell receptor beta locus.

enriched and aggregated in the TLS, indicating the potential role of TLS in priming non-sentinel LN derived clones. To collaborate the hypothesis, we co-stained PNAD (high endothelial venules marker), CD3, and CD20 and found the existence of HEV in TLS indicating the possibility of naive T cell infiltrating tumors from the circulation (online supplemental figure S4A). In addition, we performed costaining of CD103 (DC marker), CD8, and PD1 in the primary breast tumor to show the colocalization of antigen presenting cells and activated T cells (online supplemental figure S4B). The evidence supported the possibility that tumor reactive T cells can be primed in TLS of primary tumors.

DISCUSSION

Conventionally, the tumor-specific T cell clones are primed in the sentinel LNs following antigen presentation by the mature DCs, and migrate thereafter to the tumor.[2] In this study, we found that 10.91% of the expanded T cell clones in primary tumors were not present in the sentinel LNs, whereas all expanded T cell clones in the latter were shared with the tumor site. This suggests that novel intratumoral T cell clones are antigen-primed and elicited within the tumor. However, we cannot exclude the possibility that these clones may be primed in distant LNs and migrate to tumor bed, despite little evidence supporting this hypothesis. Another possibility is that these clones might be primed in bone marrow and move to tumor. Several studies have indicated that tumor antigens can be released into blood and circulate to the bone marrow, where resident DCs can process and present tumor antigens to T cell and prime them.[27]

The novel T cell clones in the tumors are characterized by high tissue retention capacity (CXCR6 +ITGAE+) and dysfunctional tendencies (CD39 +NKG2A+CTLA4+) compared with the clones common to both primary tumors and sentinel LNs. The high tissue retention is in line with the hypothesis that the novel clones are educated and elicited in the primary tumor. CD39 and NKG2A are newly identified immune checkpoint molecules. CD39 inhibits T cell function in the tumors by converting ATP to the immunomodulatory adenosine.[22] NKG2A is coexpressed with the tissue-resident molecule CD103 on the T cells, and inhibits their function on binding with the HLA-E receptor.[23] The high expression levels of both receptors indicated that the novel T cell clones elicited in the tumor have divergent coinhibitory patterns compared with the conventional anticancer T

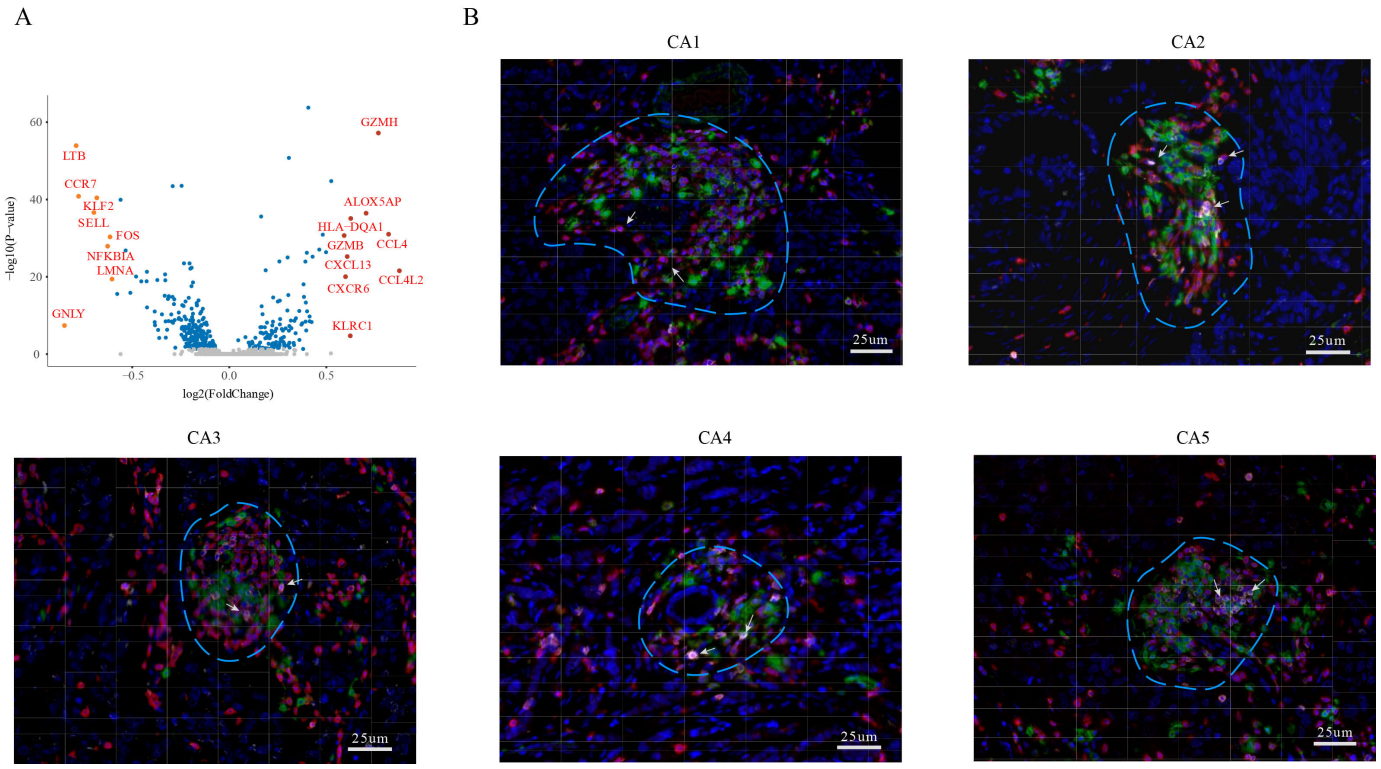

Figure 6 The TLS in primary breast cancer may induce intratumoral novel T cell clones. (A) DEGs between expanded clonal CD8 T cells and antigen-experienced non-clonal CD8 T cells. Significant DEGs were screened by p<0.05 and avg_FC>=1.5. (B) Multiplex immunofluorescence imaging of tumor tissues. Red - CD3+, white - CCL4+. CD3 +CCL4+ is the signature of clonal effector T cells. Green - CD20 +B cells. The aggregation of T and B cells represents TLS. CA, cancer; DEGs, differentially expressed genes; TLS, tertiary lymphoid structures.

cells that migrate from the LNs, providing a new strategy to reinvigorate anticancer immunity.

The novel T cell clones within tumor can be non-sentinel LN derived T cells, which suggests that sentinel LN-like structures may exist within the tumor that can prime, activate and expand naïve T cells. The tumor microenvironment receives immune cells from the peripheral blood as well as the LNs.

When the blood circulation carries plenty of naïve T cells through the tumor environment, the ones with suitable binding affinity with tumor antigen can be activated, primed and reside within sentinel LN like structure.

The naïve T cells introduced by the circulating blood includes the ones with suitable binding affinity with tumor antigen, which are then retained, primed and activated within these sentinel LN like structures. Recent studies have shown that the presence of TLS in tumors increases the efficacy of cancer immunotherapy.[5 28] Based on our findings, we hypothesize that the TLS function as sentinel LN-like structures that elicit an antitumor T cell response. The successful priming of antitumor T cells largely depends on the function of DCs.[2 29 30] Although TLS in the tumors can potentially prime T cells, the role of DC maturation in this context remains to be elucidated. Future studies should focus on the factors that are essential for priming tumor-specific T cells within the tumor. In addition, our study cannot exclude other possibilities that those intratumoral novel tumor reactive T cell clones came from neither intratumoral sites nor draining LNs. For example, the tumor antigens can be released into peripheral blood, where antigen presenting cells can process and present tumor antigens to T cell and prime them, then the tumor reactive T cells retain and reside in primary tumors via peripheral blood circulation.

Conclusion

By integrative analysis of single-cell gene expression and immune profiling, our study revealed that all expanded clones identified in the sentinel LN were also present in the primary breast tumors while 10.91% of the expanded clones in the primary tumors were not found in the sentinel LNs, and these novel intratumoral T cell clones were characterized by high tissues retention capacity (CXCR6 +ITGAE+) and a distinct coinhibitory pattern (CD39 +NKG2A+) compared with the expanded T cell clones common to both sites. Multiplex immunofluorescence imaging showed the TLSs may play a role in eliciting non-sentinel LN-derived T cell clones. These results point to the need for exploring the role of TLS in antitumor immunity.

Author affiliations
[1]Department of Hepatobiliary Surgery, Nanjing University Medical School Affiliated Nanjing Drum Tower Hospital, Nanjing, Jiangsu, China
[2]Department of Pathology, Harbin Medical University, Harbin, Heilongjiang, China
[3]Department of Breast Surgery, Harbin Medical University Cancer Hospital, Harbin, Heilongjiang, China

[4]Translational Medicine Research and Cooperation Center of Northern China, Heilongjiang Academy of Medical Sciences, Harbin, Heilongjiang, China
[5]Sino-Russian Medical Research Center, Harbin Medical University, Harbin, People's Republic of China

Acknowledgements We thank the Sugon Advanced Computing service platform and Suzhou Supercomputing Center for providing the HPC environment.

Contributors Conceived project: SJ; performed experiments and collected data: all authors; analyzed data: SJ and QX; acquired funding: SJ, DPa nd TL; wrote manuscript: SJ and QX; guarantor: SJ.

Funding This work was supported by grants from Key Research Program of the Science and Technology Department of Jiangsu Province (BE2021602 to SJ), The Key Project of the Ministry of Science and Technology of China (SQ2021YFA090185 to SJ), The Key Project by Medical Science and Technology Development Foundation, Nanjing Department of Health (ZKX2020001 to SJ), National Natural Science Foundation of China (82072903 to TL), National Natural Science Foundation of China (81972706 to TL), Heilongjiang Province Natural Science Foundation Joint Guidance Project (LH2020H125 to TL), and Heilongjiang Province Returned Personnel Funding (21032190029 to TL).

Competing interests None declared.

Patient consent for publication Not applicable.

Ethics approval The study was conducted in accordance with the Declaration of Helsinki. Ethical approval was obtained from the Research Ethics Committee of Harbin Medical University Cancer Hospital.

Provenance and peer review Not commissioned; externally peer reviewed.

Data availability statement Data are available in a public, open access repository. All raw scRNA-seq and scTCR-seq will be deposited to GEO shortly, and the accession number will be provided when available.

ORCID iD
Shiping Jiao http://orcid.org/0000-0001-6546-9369

REFERENCES

1 Long B, Brém E, Koyfman A. Oncologic emergencies: immune-based cancer therapies and complications. *West J Emerg Med* 2020;21:566–80.
2 Mellman I, Coukos G, Dranoff G. Cancer immunotherapy comes of age. *Nature* 2011;480:480–9.
3 Sautès-Fridman C, Petitprez F, Calderaro J, *et al*. Tertiary lymphoid structures in the era of cancer immunotherapy. *Nat Rev Cancer* 2019;19:307–25.
4 Hollern DP, Xu N, Thennavan A, *et al*. B cells and T follicular helper cells mediate response to checkpoint inhibitors in high mutation burden mouse models of breast cancer. *Cell* 2019;179:e1121:1191–206.
5 Cabrita R, Lauss M, Sanna A, *et al*. Tertiary lymphoid structures improve immunotherapy and survival in melanoma. *Nature* 2020;577:561–5.
6 Petitprez F, de Reyniès A, Keung EZ, *et al*. B cells are associated with survival and immunotherapy response in sarcoma. *Nature* 2020;577:556–60.
7 Jiao S, Subudhi SK, Aparicio A, *et al*. Differences in tumor microenvironment dictate T helper lineage polarization and response to immune checkpoint therapy. *Cell* 2019;179:e1113:1177–90.
8 Xiong Q, Peng C, Yan X, *et al*. Characteristics of SARS-CoV-2-specific cytotoxic T cells revealed by single-cell immune profiling of longitudinal COVID-19 blood samples. *Signal Transduct Target Ther* 2020;5:285.
9 Yost KE, Satpathy AT, Wells DK, *et al*. Clonal replacement of tumor-specific T cells following PD-1 blockade. *Nat Med* 2019;25:1251–9.
10 Waks AG, Winer EP. Breast cancer treatment: a review. *JAMA* 2019;321:288–300.
11 Stuart T, Butler A, Hoffman P, *et al*. Comprehensive integration of single-cell data. *Cell* 2019;177:1888–902.
12 Yost KE, Satpathy AT, Wells DK, *et al*. Clonal replacement of tumor-specific T cells following PD-1 blockade. *Nat Med* 2019;25:1251–9.
13 Bergen V, Lange M, Peidli S, *et al*. Generalizing RNA velocity to transient cell states through dynamical modeling. *Nat Biotechnol* 2020;38:1408–14.
14 La Manno G, Soldatov R, Zeisel A, *et al*. RNA velocity of single cells. *Nature* 2018;560:494–8.
15 Makki J. Diversity of breast carcinoma: histological subtypes and clinical relevance. *Clin Med Insights Pathol* 2015;8:23–31.
16 Patel AP, Tirosh I, Trombetta JJ, *et al*. Single-cell RNA-seq highlights intratumoral heterogeneity in primary glioblastoma. *Science* 2014;344:1396–401.
17 Puram SV, Tirosh I, Parikh AS, *et al*. Single-cell transcriptomic analysis of primary and metastatic tumor ecosystems in head and neck cancer. *Cell* 2017;171:1611–24.
18 Tirosh I, Izar B, Prakadan SM, *et al*. Dissecting the multicellular ecosystem of metastatic melanoma by single-cell RNA-seq. *Science* 2016;352:189–96.
19 Tian T, Li X, Hua Z, *et al*. S100A7 promotes the migration, invasion and metastasis of human cervical cancer cells through epithelial-mesenchymal transition. *Oncotarget* 2017;8:24964–77.
20 Srikrishna G. S100A8 and S100A9: new insights into their roles in malignancy. *J Innate Immun* 2012;4:31–40.
21 Zhang Y, Zheng L, Zhang L, *et al*. Deep single-cell RNA sequencing data of individual T cells from treatment-naïve colorectal cancer patients. *Sci Data* 2019;6:131.
22 Li X-Y, Moesta AK, Xiao C, *et al*. Targeting CD39 in cancer reveals an extracellular ATP- and Inflammasome-Driven tumor immunity. *Cancer Discov* 2019;9:1754–73.
23 van Montfoort N, Borst L, Korrer MJ, *et al*. NKG2A blockade potentiates CD8 T cell immunity induced by cancer vaccines. *Cell* 2018;175:1744–55.
24 Chambers CA, Kuhns MS, Egen JG, *et al*. CTLA-4-mediated inhibition in regulation of T cell responses: mechanisms and manipulation in tumor immunotherapy. *Annu Rev Immunol* 2001;19:565–94.
25 Colpitts SL, Dalton NM, Scott P. Il-7 receptor expression provides the potential for long-term survival of both CD62Lhigh central memory T cells and Th1 effector cells during Leishmania major infection. *J Immunol* 2009;182:5702–11.
26 van der Leun AM, Thommen DS, Schumacher TN. CD8$^+$ T cell states in human cancer: insights from single-cell analysis. *Nat Rev Cancer* 2020;20:218–32.
27 Schirrmacher V, Feuerer M, Fournier P, *et al*. T-cell priming in bone marrow: the potential for long-lasting protective anti-tumor immunity. *Trends Mol Med* 2003;9:526–34.
28 Helmink BA, Reddy SM, Gao J, *et al*. B cells and tertiary lymphoid structures promote immunotherapy response. *Nature* 2020;577:549–55.
29 Mellman I, Steinman RM. Dendritic cells: specialized and regulated antigen processing machines. *Cell* 2001;106:255–8.
30 Trombetta ES, Mellman I. Cell biology of antigen processing in vitro and in vivo. *Annu Rev Immunol* 2005;23:975–1028.

Supplementary information

The online version contains supplementary material.

Additional file 1: Table S1. Clinical characteristics of breast cancer patients.

Additional file 2: Table S2. Mapping statistics of samples.

Additional file 3. Table S3. Differentially expressed genes between clusters.

Additional file 4. Table S4. Differentially expressed genes between T cell clusters.

Figure S1. Primary cancer cells inclined to metastasis express high levels of S100A and APOD. A) Density of the number of UMIs, number of genes and percentage of mitochondrial counts. B) UMAP of all cells color-coded by sample. C) Sample percentage in each cluster. D) Sample percentage in CA and LN for each cluster. E) Violin plot of epithelial scores in each cluster. F) CNV heatmap of reference cells and malignant cells. G) Percentage of cancer cells of each sample in each cluster, and percentage of CA and LN cancer cells in each cluster.

Figure S2. Characteristics of T cells residing in primary breast cancers and paired sentinel LNs. A) Violin plot of nFeature_RNA, nCount_RNA, and percent.mt of T cells. B) UMAP of T cells color-coded by samples. C) Percentage of T cells of each sample in each cluster. D) Percentage of T cells of each sample for CA and LN in each cluster.

Jiao S, *et al. J Immunother Cancer* 2022; 10:e003325. doi: 10.1136/jitc-2021-003325

Figure S3. Tumor reactivity of expanded T cell clones and non-expanded T cell clones. A) The details of TCR sequences used in the assays were presented. B) Patient autologous CD8 T cells transduced with TCR sequences were cultured alone or with autologous tumor cells, and IFNγ in the suppernant was measured by ELISA.

Figure S4. The presence of high endothelial venules and the co-localization of antigen presenting cells and activated T cells. Multiplex immunofluorescence imaging of tumor tissues. A) Yellow – PNAD+, purple – CD20+, green – CD3+, blue – DAPI. The staining was performed in sentinel lymph node as positive control of PNAD (HEV marker) and 2 primary breast tumors. B) Red – CD8+, white – CD103+, green – PD1+, blue – DAPI. The staining was performed in primary breast tumor.

Jiao S, *et al. J Immunother Cancer* 2022; 10:e003325. doi: 10.1136/jitc-2021-003325

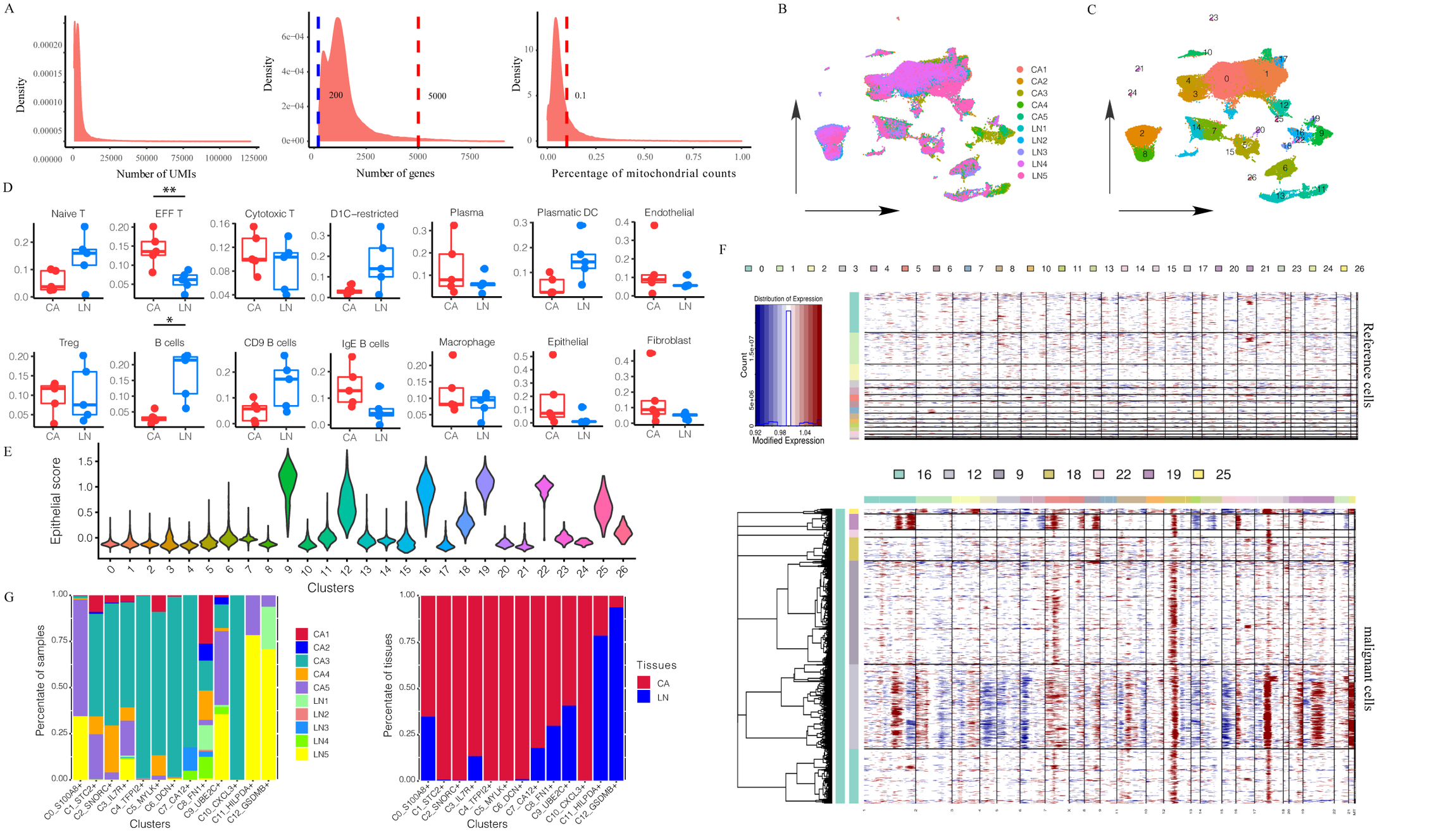
A
Density
Number of UMIs
Number of genes
200
5000
Percentage of mitochondrial counts
0.1
B
CA1
CA2
CA3
CA4
CA5
LN1
LN2
LN3
LN4
LN5
C
D
Naive T
EFF T
Cytotoxic T
D1C−restricted
Plasma
Plasmatic DC
Endothelial
Treg
B cells
CD9 B cells
IgE B cells
Macrophage
Epithelial
Fibroblast
CA
LN
E
Epithelial score
Clusters
F
Distribution of Expression
Count
Modified Expression
Reference cells
malignant cells
G
Percentate of samples
Percentate of tissues
Tissues
C0_S100A8+
C1_STC2+
C2_SNORC+
C3_IL7R+
C4_TFPI2+
C5_MYLK+
C6_DCN+
C7_CA12+
C8_FN1+
C9_UBE2C+
C10_CXCL3+
C11_HILPDA+
C12_GSDMB+

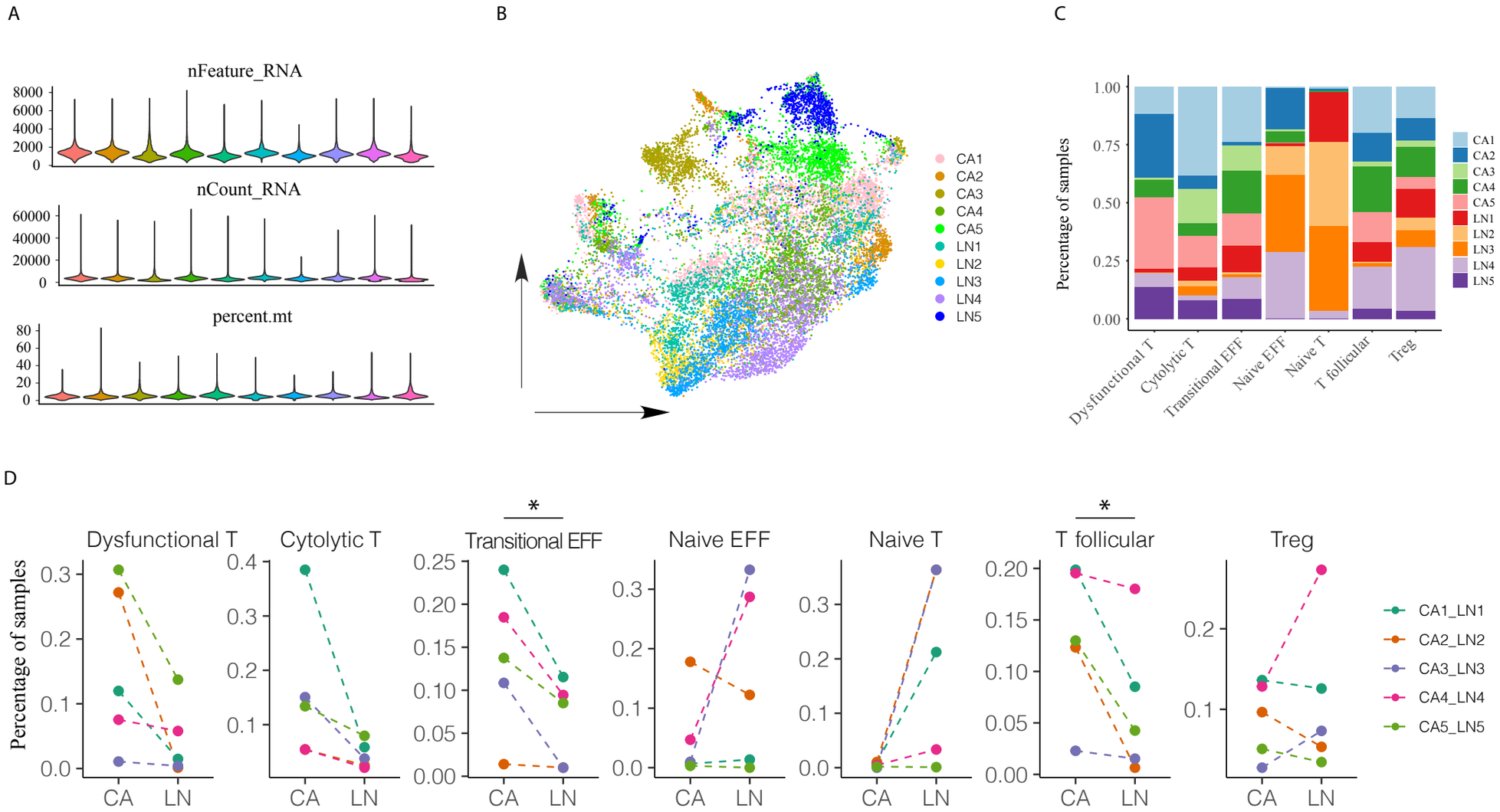
A
nFeature_RNA
8000
6000
4000
2000
0
nCount_RNA
60000
40000
20000
0
percent.mt
80
60
40
20
0
B
CA1
CA2
CA3
CA4
CA5
LN1
LN2
LN3
LN4
LN5
C
Percentage of samples
1.00
0.75
0.50
0.25
0.00
Dysfunctional T
Cytolytic T
Transitional EFF
Naive EFF
Naive T
T follicular
Treg
D
Percentage of samples
Dysfunctional T
Cytolytic T
Transitional EFF
Naive EFF
Naive T
T follicular
Treg
*
*
CA
LN
CA1_LN1
CA2_LN2
CA3_LN3
CA4_LN4
CA5_LN5

A

Clonotype	CDR3_aa	V_gene	J_gene	Consensus
TCR-1_TRA	CALLLGVDYKLSF	TRAV9-2	TRAJ20	L*FLHVKDQDHYLGNTLKMNYSPGLVSLILLLLGRTRGDSVTQMEGPVTLSEEACLTINCTYTATGYPSLFWYVQYP GEGLQLLLKATKADDKGSNKGFEATYRKETTSFHLEKGSVQVSDSAVYFCALLGVDYKLSFGAGTTVTVRANIQNP DPAVYQLRDX
TCR-1_TRB	CASMEGTARDGYTF	TRBV6-1	TRBJ1-2	VPLSPMHRPRRPLHPVAPAMSIGLLCCVAFSLLWASPVNAGVTQTPKFQVLKTGQSMTLQCAQDMNHNSMYWY RQDPGMGLRLIYYSASEGTTDKGEVPNGYNVSRLNKREFSLRLESAAPSQTSVYFCASMEGTARDGYTFGSGTRL TVVEDLNKVFPPEVAVFEPSX
TCR-2_TRA	CAVINFNKFYF	TRAV12-2	TRAJ21	KADSFYDF*SRNIHSRCIF*GFKI*ILSEPGQRRMMKSLRVLLVILWLQLSWVWSQQKEVEQNSGPLSVPEGAIASL NCTYSDRVSQSFFWYRQYSGKSPELIMSIYSNGDKEDGRFTAQLNKASQYVSLLIRDSQPSDSATYLCAVINFNKFY FGSGTKLNVKPNIQNPDPAVYQLRDX
TCR-2_TRB	CASSLALTDTQYF	TRBV27	TRBJ2-3	PGAPRTGRHLPDAAMGPQLLGYVVLCLLGAGPLEAQVTQNPRYLITVTGKKLTVTCSQNMNHEYMSWYRQDPGL GLRQIYYSMNVEVTDKGDVPEGYKVSRKEKRNFPLILESPSPNQTSLYFCASSLALTDTQYFGPGTRLTVLEDLKNVF PPEVAVFEPSX
TCR-3_TRA	CAVRLRSGNTGKLIF	TRAV3	TRAJ37	GVGKHQCPEEGPFPKALC*HRVAGSSSRAHSLGWGHISSRGGLERTPPIPPAVSLAGAMASAPISMLAMLFTLSGL RAQSVAQPEDQVNVAEGNPLTVKCTYSVSGNPYLFWYVQYPNRGLQFLLKYITGDNLVKGSYGFEAEFNKSQTSF HLKKPSALVSDSALYFCAVRLRSGNTGKLIFGQGTTLQVKPDIQNPDPAVYQLRDX
TCR-3_TRB	CTSLRDTPDTQYF	TRBV29-1	TRBJ2-3	KER*T*VSLLSAFSQGRGHHLKMLSLLLLLLGLGSVFSAVISQKPSRDICQRGTSLTIQCQVDSQVTMMFWYRQQP GQSLTLIATANQGSEATYESGFVIDKFPISRPNLTFSTLTVSNLSPEDSSIYLCTSLRDTPDTQYFGPGTRLTVLEDLKN VFPPEVAVFEPSX
TCR-4_TRA	CAFGGGKLIF	TRAV13-1	TRAJ3	S*LGRTRMTSIRAVFIFLWLQLDLVNGENVEQHPSTLSVQEGDSAVIKCTYSDSASNYFPWYKQELGKRPQLIIDIRS NVGEKKDQRIAVTLNKTAKHFSLHITETQPEDSAVYFCAASWGSSASKIIFGSGTRLSIRPNIQNPDPAVYQLRDX
TCR-4_TRB	CAWSLAGAGGELFF	TRBV7-8	TRBJ2-2	DVV*GPRVQTAWEPKK*TMH**W*KADTYLKQHPSVF**KCCDPEVLGIERGSDVTVGTALWRQGRPLSSASVH SDTDLVKPPSWPDPAMGTRLLCWVVLGFLGTDHTGAGVSQSPRYKVAKRGQDVALRCDPISGHVSLFWYQQAL GQGPEFLTYFQNEAQLDKSGLPSDRFFAERPEGSVSTLKIQRTQQEDSAVYLCASSLGGELFFGEGSRLTVLEDLKN VFPPEVAVFEPSX
TCR-5_TRA	CVVSANNQGGKLIF	TRAV10	TRAJ23	GADLCRIKMKKHLTTFLVILWLYFYRGNGKNQVEQSPQSLIILEGKNCTLQCNYTVSPFSNLRWYKQDTGRGPVSLT IMTFSENTKSNGRYTATLDADTKQSSLHITASQLSDSASYICVVSANNQGGKLIFGQGTELSVKPNIQNPDPAVYQL RDX
TCR-5_TRB	CASSLDQEDNEQFF	TRBV5-6	TRBJ2-1	YLGLHTSLQLGRTGRESSVLEH*T*GRLHGEDKGQ*HHRIPLPSGKSRPRTHSALPQENQALNQMQCFLSLCAMG PGLLCWALLCLLGAGLVDAGVTQSPTHLIKTRGQQVTLRCSPKSGHDTVSWYQQALGQGPQFIFQYYEEEERQRG NFPDRFSGHQFPNYSSELNVNALLLGDSALYLCASSLDQEDNEQFFGPGTRLTVLEDLKNVFPPEVAVFEPSX
TCR-6_TRA	CAVFRGGSYIPTF	TRAV12-1	TRBJ6	GG**YTRGCENNLFFLIGRTDSFYDS*SGRNKVSLLCSFLFGLKILMLSEPGQKRMMISLRVLLVILWLQLSWVWS QRKEVEQDPGPFNVPEGATVAFNCTYSNSASQSFFWYRQDCRKEPKLLMSVYSSGNEDGRFTAQLNRASQYISLL IRDSKLSDSATYLCAVFRGGSYIPTFGRGTSLIVHPYIQNPDPAVYQLRDX
TCR-6_TRB	CASSFSGNTEAFF	TRBV6-5	TRBJ1-1	ESPAPLSSMHRYRRPLRHAASAMSIGLLCCAALSLLWAGPVNAGVTQTPKFQVLKTGQSMTLQCAQDMNHEYM SWYRQDPGMGLRLIHYSVGAGITDQGEVPNGYNVSRSTTEDFPLRLLSAAPSQTSVYFCASSFSGNTEAFFGQGT RLTVVEDLNKVFPPEVAVFEPSX
TCR-7_TRA	CLVGEDTGFQKLVF	TRAV1-2	TRAJ33	PT*SVYLLQTPMAQELGMQCQARGILQQMWGVFLLYVSMKMGGTTGQNIDQPTEMTATEGAIVQINCTYQTS GFNGLFWYQQHAGEAPTFLSYNVLDGLEEKGRFSSFLSRSKGYSYLLLKELQMKDSASYLCAAMDSNYQLIWGAG TKLIIKPDIQNPDPAVYQLRDX
TCR-7_TRB	CASSISYGGLAEYEQYF	TRBV20-1	TRBJ2-7	EAVVTTLPREGGVRPSRKMLLLLLLLGPGSGLGAVVSQHPSWVICKSGTSVKIECRSLDFQATTMFWYRQFPKQSL LMATSNEGSKATYEQGVEKDKFLINHASLTLSTLTVTSAHPEDSSFYICSARRLAGDSYEQYFGPGTRLTVTEDLKNV FPPEVAVFEPSX
TCR-8_TRA	CAVTPPEGGYNKLIF	TRAV12-2	TRAJ4	KADSFYDF*SRNIHSRCIF*GFKI*ILSEPGQRRMMKSLRVLLVILWLQLSWVWSQQKEVEQNSGPLSVPEGAIASL NCTYSDRVSQSFFWYRQYSGKSPELIMSIYSNGDKEDGRFTAQLNKASQYVSLLIRDSQPSDSATYLCAVTPPEGG YNKLIFGAGTRLAVHPYIQNPDPAVYQLRDX
TCR-8_TRB	CASSSTPSEQYF	TRBV5-1	TRBJ2-7	RTKP*AQTQCCLPLCAMGSRLLCWVLLCLLGAGPVKAGVTQTPRYLIKTRGQQVTLSCSPISGHRSVSWYQQTPG QGLQFLFEYFSETQRNKGNFPGRFSGRQFSNSRSEMNVSTLELGDSALYLCASSSTPSEQYFGPGTRLTVTEDLKN VFPPEVAVFEPSX

B

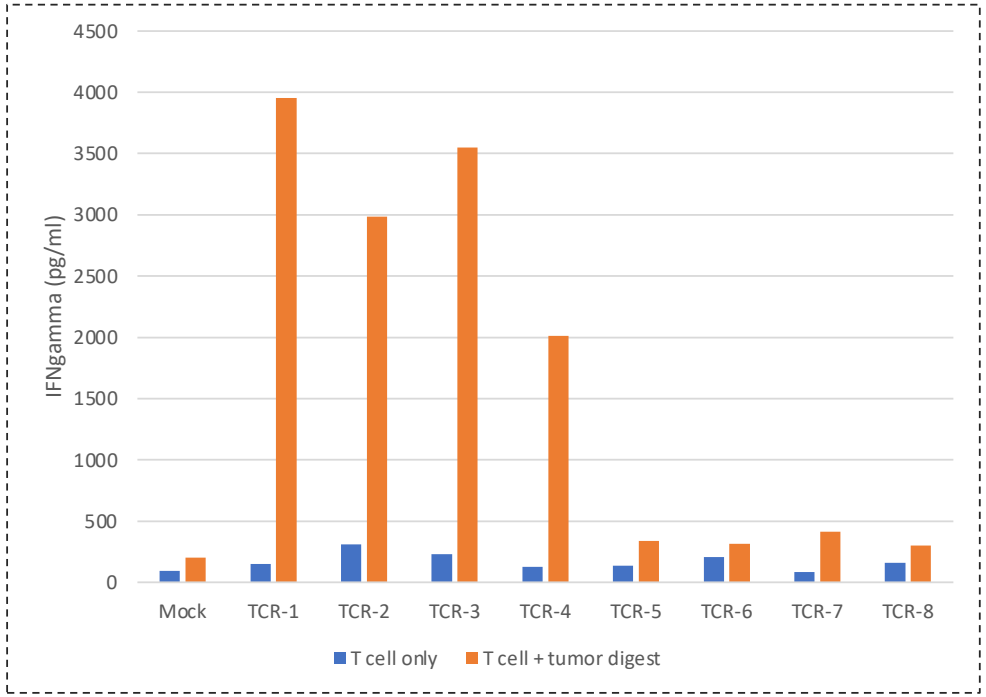

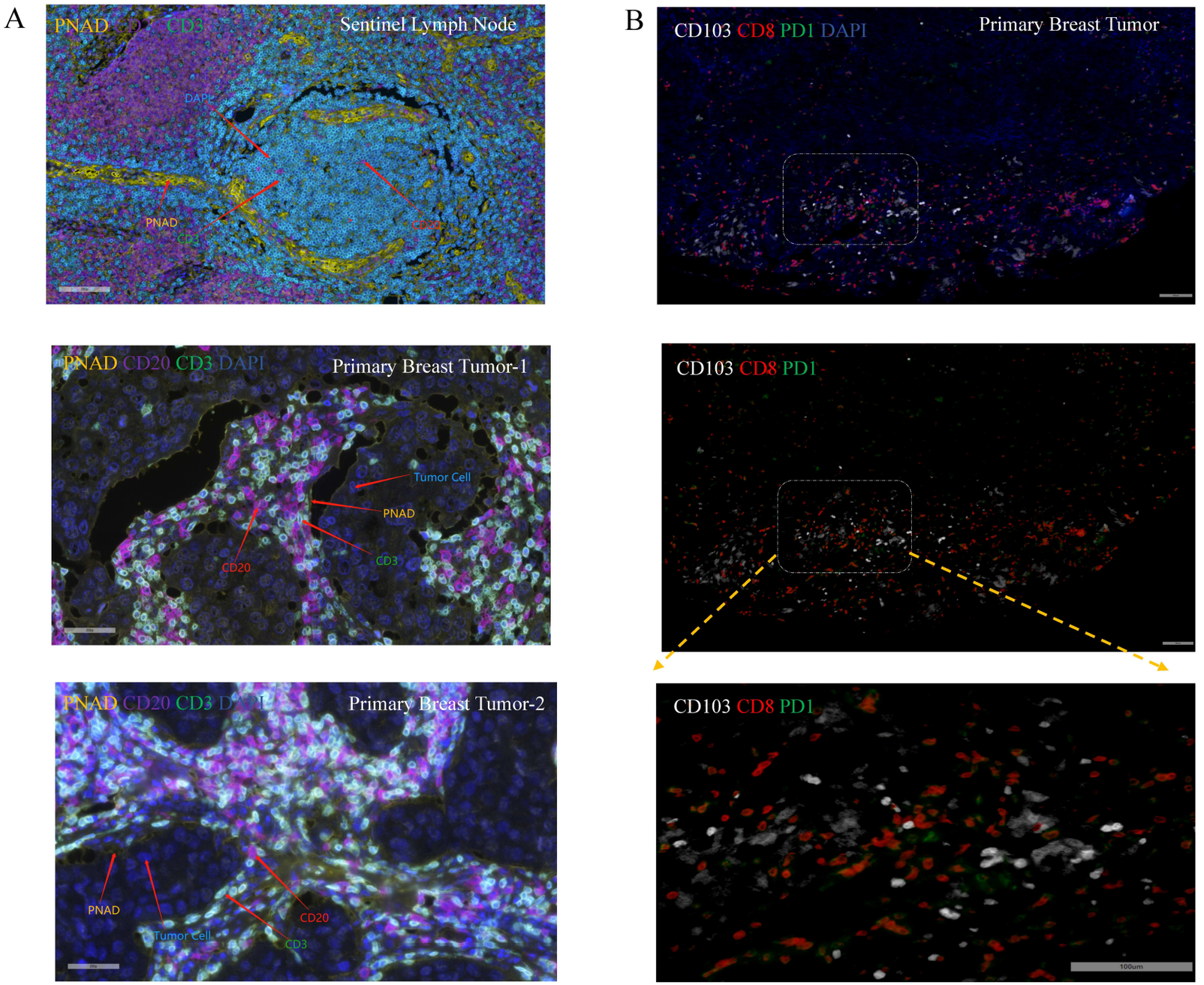
A
PNAD CD20 CD3
Sentinel Lymph Node
DAPI
PNAD
CD3
CD20
PNAD CD20 CD3 DAPI
Primary Breast Tumor-1
Tumor Cell
PNAD
CD20
CD3
PNAD CD20 CD3 DAPI
Primary Breast Tumor-2
PNAD
Tumor Cell
CD20
CD3
B
CD103 CD8 PD1 DAPI
Primary Breast Tumor
CD103 CD8 PD1
CD103 CD8 PD1
100um